

# Grounded Relational Inference: Domain Knowledge Driven Explainable Autonomous Driving

Chen Tang<sup>1,2†</sup>, Nishan Srishankar<sup>1,3†</sup>, Sujitha Martin<sup>1</sup>, Masayoshi Tomizuka<sup>2</sup>

**Abstract**—Explainability is essential for autonomous vehicles and other robotics systems interacting with humans and other objects during operation. Humans need to understand and anticipate the actions taken by the machines for trustful and safe cooperation. In this work, we aim to enable the explainability of an autonomous driving system at the design stage by incorporating expert domain knowledge into the model. We propose Grounded Relational Inference (GRI). It models an interactive system’s underlying dynamics by inferring an interaction graph representing the agents’ relations. We ensure an interpretable interaction graph by grounding the relational latent space into semantic behaviors defined with expert domain knowledge. We demonstrate that it can model interactive traffic scenarios under both simulation and real-world settings, and generate interpretable graphs explaining the vehicle’s behavior by their interactions.

**Index Terms**—intelligent transportation system, learning from demonstration, deep learning in robotics and automation, explainable AI

## I. INTRODUCTION

DEEP learning has been utilized to address various autonomous driving problems [1], [2], [3]. However, deep neural networks lack the transparency that helps people understand their underlying mechanism. It is a crucial drawback for safety-critical applications with humans involved (e.g., autonomous vehicles). Humans need to understand and anticipate the actions taken by the machines for trustful and safe cooperation. In response to this problem, the concept of explainable AI (XAI) was introduced. It refers to machine learning techniques that provide details and reasons that make a model’s mechanism easy to understand [4]. Most of the existing works for deep learning models focus on post-hoc explanations [4]. They enhance model explainability by unraveling the underlying mechanisms of a trained model: Vision-based approaches, such as visual attention [5] and deconvolution [6], illustrate which segments of the input image affect the outputs; Interaction-aware models, such as social LSTM with social attention [7], [8] and graph neural networks (GNN) with graph attention [9], [10], [11], [12], identify the agents that are critical to the decision-making procedure.

Although promising, post-hoc explanations could be ambiguous and falsely interpreted by humans because of the non-interpretable nature of deep neural networks. Unless the

model is interpretable by design, it is deceiving to claim that the generated post-hoc explanation can capture the model’s underlying mechanism. In this work, we aim to improve interpretability at the design stage and develop a model that can generate interpretable explanations clearly defined in human domain knowledge and operate as the explanations suggest. We consider the problem of interactive system modeling—which is the foundation behind interaction-aware prediction and control models for autonomous vehicles—and follow the practice in Neural Relational Inference (NRI) [12] to model an interactive system by explicitly inferring its inherent interactions. Similar to NRI, our model outputs an interaction graph with discrete edge variables corresponding to a cluster of pairwise interactions between the agents. However, unlike NRI, which learns latent space in an unsupervised manner, we aim to ground it in a set of interactive behaviors defined with expert domain knowledge.

As a running example, consider the scenario depicted in Fig. 1, where we ask different models to control the red vehicle. Attention mechanisms can indicate the critical pixels or agents, but they cannot recognize different effects—the two cars are mutually important but affect each other in distinct ways. The NRI model can distinguish between different interactive behaviors. Still, the latent space does not have explicit semantic meaning. In contrast, our model should determine the interaction graph with a latent space grounded in yielding and cutting-in behaviors. It learns control policies that generate behaviors consistent with their definitions in domain knowledge (e.g., traffic rules) and executes the corresponding policies according to the inferred edge types. As a result, we ensure a semantic interaction graph, which illustrates the model’s understanding of the scenario and explains the action it takes.

A straightforward way to enable semantic relations is supervision. Interaction labels can be either obtained from human experts [13] or heuristic labeling functions [14]. However, accurate and unbiased labels are practically prohibitive because human intentions are intricate and unobservable. Inaccurate labels could introduce bias and limit model capacity. Moreover, it is unclear if the model can understand the semantic meaning behind the labels and synthesize the right behaviors. Instead, we recast relational inference into an inverse reinforcement learning (IRL) problem and introduce structured reward functions to ground the latent space. Concretely, the system is modeled as a multi-agent Markov decision process (MDP), where the agents share a reward function that depends on the relational latent space. We design structured reward functions based on expert domain knowledge to explicitly

<sup>1</sup> Honda Research Institute, CA, USA

<sup>2</sup> Department of Mechanical Engineering, University of California Berkeley, CA, USA

<sup>3</sup> Department of Robotics Engineering, Worcester Polytechnic Institute, MA, USA

† Work done during internship at Honda Research Institute.

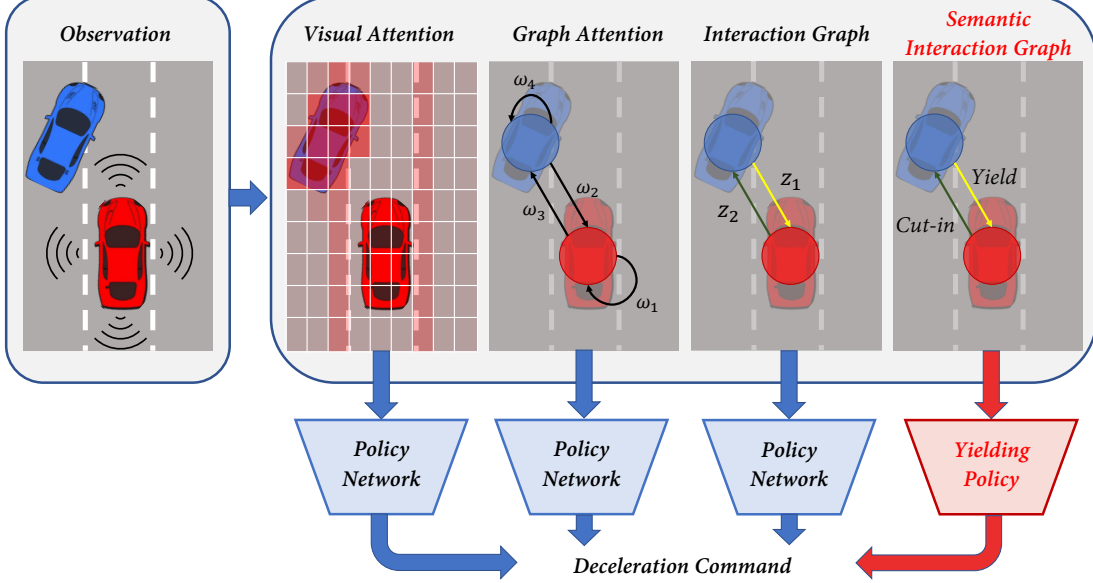


Fig. 1: A motivating lane-changing scenario where we ask different models to control the red vehicle. All the models generate deceleration commands but have different intermediate outputs. With the aid of visual attention, we generate a heat map indicating the critical pixels of the input image. Graph attention network assigns edge weights  $\omega_i$  to specify the importance of surrounding vehicles to the controlled vehicle. However, the attention mechanisms cannot recognize different effects—the two cars are mutually important but affect each other in distinct ways. The NRI model can distinguish between different interactive behaviors by assigning different values to the latent variables  $z_i$  in the interaction graph. Still, the latent space does not have explicit semantic meaning. In contrast, our model ensures a semantic interaction graph, which illustrates the model’s understanding of the scenario and explain the action it takes. It determines the interaction graph with a latent space grounded in yielding and cutting-in behaviors. It learns control policies that generate behaviors consistent with their definitions in domain knowledge (e.g., traffic rules) and executes the corresponding policies according to the inferred edge types.

define the interactive behaviors corresponding to the latent space. Compared to direct supervision, we merely specify the function space of the reward for each type of interaction, but leave the reward parameters and interaction graph—namely which reward function each agent follows—to be learned from data without supervision signals.

To solve the formulated IRL problem, we propose Grounded Relational Inference (GRI). It has a variational-autoencoder-like (VAE) GNN in NRI [12] as the backbone model. Additionally, we incorporate the structured reward functions into the model as a decoder. A variational extension of the adversarial inverse reinforcement learning (AIRL) algorithm is derived to train all the modules simultaneously. Experiments show that GRI can model interactive traffic scenarios under simulation and real-world settings, and generate interpretable graphs explaining the vehicle’s behavior by their interactions. Moreover, the semantically meaningful latent space enables humans to govern the model and ensure safety under unfamiliar situations.

To sum up, our contributions are as follows:

- We reformulate relational inference into a multi-agent IRL problem with relational latent space and introduce structured reward functions as a systematic and principled manner to incorporate expert domain knowledge into interactive driving behavior model.
- We propose Grounded Relational Inference model to

solve the formulated multi-agent IRL problem. It learns to infer the agents’ relations and model the underlying dynamics of the interactive system based on a semantic relational latent space grounded by domain knowledge.

- We apply the proposed framework to some simple traffic scenarios in both simulation and real-world setting for evaluation. We show that the interaction graphs inferred by GRI have explicit semantic meanings and therefore improves the explainability of the overall model.

## II. RELATED WORK

Our model combines graph neural networks and adversarial inverse reinforcement learning for interactive system modeling. This section gives a concise review on these two topics and summarizes the existing works closely related to ours. We also discuss some additional works on explainable driving models as a complement to the discussion in Sec. I.

**Interaction modeling using GNN.** GNN has been widely applied for interactive system modeling in recent years [11], [15], [16]. One category of models we find particularly interesting is those with graph attention mechanism. One seminal work is Graph Attention Network (GAT) [10] which performed well on large-scale inductive classification problems. VAIN [9] applied attention in multi-agent modeling. The attention map unravels the interior interaction structure to some extent which improves the explainability of VAIN. An

approach closely related to ours is NRI [12], which modeled the interaction structure explicitly with discrete relational latent space compared to the continuous graph attention. We explain the difference between NRI and our proposed method in Sec. I and V. Another related approach in the autonomous driving domain is [14], which also modeled interactive driving behavior with semantically meaningful interactions but in a supervised manner.

**Adversarial inverse reinforcement learning.** Our work is related to two types of IRL methods: multi-agent and latent AIRL algorithms. Yu et al. [17] proposed a multi-agent AIRL framework for Markov games under correlated equilibrium. It is capable of modeling general heterogeneous multi-agent interactions. The PS-GAIL algorithm [18] considered a multi-agent environment in the driving domain that is similar to ours—homogeneous agents with shared policy under centralized control—and extended GAIL [19] to model the interactive behaviors. In [20], they augmented the reward in PS-GAIL as a principle manner to specify prior knowledge, which shares the same spirit with the structured reward functions in GRI. Latent AIRL models integrate a VAE into either the discriminator or the generator for different purposes. Wang et al. [21] conditioned the discriminator on the embeddings generated by a VAE trained separately using behavior cloning. The VAE encodes trajectories into low-dimensional space, enabling the generator to produce diverse behaviors from limited demonstration. VDB [22] constrained information contained in the discriminator’s internal representation to balance the training procedure for adversarial learning algorithms. The PEMIRL framework [23] achieved meta-IRL by encoding demonstration into a contextual latent space. Though studied in different context, PEMIRL is conceptually similar to our framework as both its generator and discriminator depend on the inferred context variables.

**Explainable Autonomous Driving.** At the end of this section, we discuss some additional works related to explainable autonomous driving as a complement to those we have mentioned in Sec. I. They addressed some shortcomings of the discussed approaches, especially those methods based on attention mechanisms. Kim et al. [24] trained a textual explanation generator concurrently with a visual-attention-based controller in a supervised manner. It generates sentences explaining the control action as a consequence of certain objects highlighted in the attention map, which can be easily interpreted compared to visual attention. Another issue of attention that has been raised in the literature is causal confusion [25]. The model does not necessarily assign high attention weights to objects/regions that influence the control actions. In [5], a fine-grained decoder was proposed to refine visual attention maps and detect critical regions through causality tests. In [26], Li et al. adopted a similar idea for object-level reasoning. Causal inference was applied to identify risk objects in driving scenes. One interesting observation was that the detection accuracy was improved with intervention during the training stage, i.e., augmenting the training data by masking out non-causal objects. However, intervention requires explicit prior knowledge on the causal relations to label the causal and non-causal objects in a scene. Similar to intention labels,

such kind of labels is generally prohibitive due to the intricate nature of human cognition.

### III. BACKGROUND

In this section, we would like to briefly summarize two algorithms that are closely related to our approach, in order to prepare the readers for the core technical content.

#### A. Neural Relational Inference (NRI)

Kipf et al. [12] represent an interacting system with  $N$  objects as a complete bi-directed graph  $\mathcal{G}_{\text{scene}} = (\mathcal{V}, \mathcal{E})$  with vertices  $\mathcal{V} = \{v_i\}_{i=1}^N$  and edges  $\mathcal{E} = \{e_{i,j} = (v_i, v_j) \mid i \neq j\}$ . The edge  $e_{i,j}$  refers to the one pointing from the vertex  $v_i$  to  $v_j$ . Each vertex corresponds to an object in the system. The NRI model is formalized as a VAE with a GNN encoder inferring the underlying interactions and a GNN decoder synthesizing the system dynamics given the interactions.

Formally, the model aims to reconstruct a given state trajectory, denoted by  $\mathbf{x} = (\mathbf{x}^0, \dots, \mathbf{x}^{T-1})$ , where  $T$  is the number of timesteps and  $\mathbf{x}^t = \{\mathbf{x}_1^t, \dots, \mathbf{x}_N^t\}$ . The vector  $\mathbf{x}_i^t \in \mathbb{R}^n$  denotes the state vector of object  $v_i$  at time  $t$ . Alternatively, the trajectory can be decomposed into  $\mathbf{x} = (\mathbf{x}_1, \dots, \mathbf{x}_N)$ , where  $\mathbf{x}_i = \{\mathbf{x}_i^0, \dots, \mathbf{x}_i^{T-1}\}$ . The encoder operates over  $\mathcal{G}_{\text{scene}}$ , with  $\mathbf{x}_i$  as the node feature of  $v_i$ . It infers the posterior distribution of the edge type  $z_{i,j}$  for all the edges, collected into a single vector  $\mathbf{z}$ . The decoder operates over an interaction graph  $\mathcal{G}_{\text{interact}}$  and reconstructs  $\mathbf{x}$ . The graph  $\mathcal{G}_{\text{interact}}$  is constructed by assigning sampled  $\mathbf{z}$  to the edges of  $\mathcal{G}_{\text{scene}}$  and assigning the initial state to the nodes of  $\mathcal{G}_{\text{scene}}$ . If  $\mathcal{G}_{\text{interact}}$  represents the interactions sufficiently, the decoder should be able to reconstruct the trajectory accurately.

The model is trained by maximizing the evidence lower bound (ELBO):

$$\mathcal{L} = \mathbb{E}_{q_\phi(\mathbf{z}|\mathbf{x})} [\log p_\gamma(\mathbf{x}|\mathbf{z})] - D_{KL} [q_\phi(\mathbf{z}|\mathbf{x}) \parallel p(\mathbf{z})],$$

where  $q_\phi(\mathbf{z}|\mathbf{x})$  is the encoder output which can be factorized as:

$$q_\phi(\mathbf{z}|\mathbf{x}) = \prod_{i=1}^N \prod_{j=1, j \neq i}^N q_\phi(z_{i,j}|\mathbf{x}), \quad (1)$$

where  $\phi$  refers to the parameters of the encoder. The decoder output  $p_\gamma(\mathbf{x}|\mathbf{z})$  can be written as:

$$p_\gamma(\mathbf{x}|\mathbf{z}) = \prod_{t=0}^{T-1} p_\gamma(\mathbf{x}^{t+1}|\mathbf{x}^t, \dots, \mathbf{x}^0, \mathbf{z}),$$

where  $\gamma$  refers to the parameters of the decoder.

#### B. Adversarial Inverse Reinforcement Learning (AIRL)

The AIRL algorithm follows the principle of maximum entropy IRL [27]. Consider a MDP defined by  $(\mathcal{X}, \mathcal{A}, \mathcal{T}, r)$ , where  $\mathcal{X}, \mathcal{A}$  are the state space and action space respectively. In the rest of the paper, we use  $\mathbf{x}$  and  $\mathbf{a}$  with any superscript or subscript to represent a state and action in  $\mathcal{X}$  and  $\mathcal{A}$ .  $\mathcal{T}$  is the transition operator given by  $\mathbf{x}_{t+1} =$

$f(\mathbf{a}_t, \mathbf{x}_t)$ <sup>1</sup>, and  $r : \mathcal{X} \times \mathcal{A} \rightarrow \mathbb{R}$  is the reward function. The maximum entropy IRL framework assumes a suboptimal expert policy  $\pi^E(\mathbf{a}|\mathbf{x})$ . The demonstration trajectories generated with the expert policy,  $\mathcal{D}^E = \{\tau_1^E, \dots, \tau_M^E\}$  where  $\tau_i^E = (\mathbf{x}_i^{E,0}, \mathbf{a}_i^{E,0}, \dots, \mathbf{x}_i^{E,T-1}, \mathbf{a}_i^{E,T-1})$ , have probabilities increasing exponentially with the cumulative reward. Concretely, they follow a Boltzmann distribution:

$$\tau_i^E \sim \pi^E(\tau) = \frac{1}{Z} \exp \left( \sum_{t=0}^{T-1} r_\lambda(\mathbf{x}_t, \mathbf{a}_t) \right),$$

where  $r_\lambda$  is the reward function with parameters denoted by  $\lambda$ . Maximum entropy IRL aims to infer the underlying reward function parameters of the expert policy. It is formalized as a maximum likelihood problem:

$$\lambda^* = \arg \max_{\lambda} \mathbb{E}_{\tau^E \sim \pi^E(\tau)} \left[ \sum_{t=0}^{T-1} r_\lambda(\mathbf{x}_t^E, \mathbf{a}_t^E) \right] - \log Z.$$

To derive a feasible algorithm to solve the problem, we need to estimate the partition function  $Z$ . One practical solution is co-training a policy model with the current estimated reward function through reinforcement learning [28]. Finn et al. [29] found the equivalency between it and a special form of the generative adversarial network (GAN). The policy model is the generator, whereas a structured discriminator is defined with the reward function to distinguish a generated trajectory  $\tau^G$  from a demonstrated one  $\tau^E$ . Fu et al. [30] proposed the AIRL algorithm based on it, using a discriminator that identifies generated samples based on the pairs of state and action instead of the entire trajectory to reduce variance:

$$\mathcal{D}_{\lambda, \eta}(\mathbf{x}, \mathbf{a}) = \frac{\exp \{r_\lambda(\mathbf{x}, \mathbf{a})\}}{\exp \{r_\lambda(\mathbf{x}, \mathbf{a})\} + \pi_\eta(\mathbf{a}|\mathbf{x})}, \quad (2)$$

where  $\pi_\eta(\mathbf{a}|\mathbf{x})$  is the policy model with parameters denoted by  $\eta$ . The models  $\mathcal{D}_{\lambda, \eta}$  and  $\pi_\eta$  are trained adversarially by solving the following min-max optimization problem:

$$\begin{aligned} \min_{\eta} \max_{\lambda} & \mathbb{E}_{\mathbf{x}^E, \mathbf{a}^E \sim \pi^E(\mathbf{x}, \mathbf{a})} [\log (\mathcal{D}_{\lambda, \eta}(\mathbf{x}^E, \mathbf{a}^E))] \\ & + \mathbb{E}_{\mathbf{x}^G, \mathbf{a}^G \sim \pi_\eta(\mathbf{x}, \mathbf{a})} [\log (1 - \mathcal{D}_{\lambda, \eta}(\mathbf{x}^G, \mathbf{a}^G))], \end{aligned} \quad (3)$$

where  $\pi^E(\mathbf{x}, \mathbf{a})$  denotes the distribution of state and action induced by the expert policy, and  $\pi_\eta(\mathbf{x}, \mathbf{a})$  is the distribution induced by the learned policy.

#### IV. PROBLEM FORMULATION

Our GRI model grounds the relational latent space in a clustering of interpretable interactions by reformulating the relational inference problem into a multi-agent IRL problem. Since the framework has the potential to be generalized to interactive systems in other domains apart from autonomous driving, we will introduce our approach in a general tone. However, it should be aware that we limit our discussion in this paper to autonomous driving problems, without claiming that it can be directly applied to other domains. GRI relies on expert

<sup>1</sup>The transition is assumed deterministic to simplify the notation. A more general form of the algorithm can be derived for stochastic systems, which is essentially the same with the deterministic case.

domain knowledge to identify all possible semantic behaviors and design the corresponding reward functions. There exists a broad range of literature on interactive driving behavior modeling [13], [31], which we can refer to when designing the rewards. We can extend the proposed framework to other fields if proper domain knowledge is available, which is left for future investigation.

We start with modeling the interactive system as a multi-agent MDP with graph representation. As in NRI, the system has an underlying interaction graph  $\mathcal{G}_{\text{interact}}$ . The discrete latent variable  $z_{i,j}$  takes a value from  $0, 1, \dots, K-1$ , where  $K$  is the number of interactions. It indicates the type of relation between  $v_i$  and  $v_j$  in respect to its effect on  $v_j$ . Additionally, we assume the objects of the system are homogeneous intelligent agents who make decisions based on their interactions with others.

Concretely, each of them is modeled with identical state space  $\mathcal{X}$ , action space  $\mathcal{A}$ , transition operator  $\mathcal{T}$  and reward function  $r : \mathcal{X} \times \mathcal{A} \rightarrow \mathbb{R}$ . At time step  $t$ , the reward of agent  $v_j$  depends on the states and actions of itself and the pairwise interactions between itself and all its neighbors:

$$\begin{aligned} r_{\xi, \psi}(v_j^t, \mathbf{z}_j) &= r_\xi^n(\mathbf{x}_j^t, \mathbf{a}_j^t) \\ &+ \sum_{i \in \mathcal{N}_j} \sum_{k=1}^K \mathbf{1}(z_{i,j} = k) r_{\psi_k}^{e,k}(\mathbf{x}_i^t, \mathbf{a}_i^t, \mathbf{x}_j^t, \mathbf{a}_j^t), \end{aligned} \quad (4)$$

where  $\mathbf{z}_j$  is the collection of  $\{z_{i,j}\}_{i \in \mathcal{N}_j}$ ,  $r_\xi^n$  is the node reward function parameterized by  $\xi$ ,  $\mathcal{N}_j$  is the set of  $v_j$ 's neighbouring nodes,  $\mathbf{1}$  is the indicator function, and  $r_{\psi_k}^{e,k}$  is the edge reward function parameterized by  $\psi_k$  for the  $k^{\text{th}}$  type of interaction. We utilize expert domain knowledge to design  $r_{\psi_k}^{e,k}$ , so that the corresponding interactive behavior emerges by maximizing the rewards. Particularly, the edge reward equals to zero for  $k=0$ , indicating the action taken by  $v_j$  does not depend on its interaction with  $v_i$ .

We assume the agents act cooperatively to maximize the cumulative reward of the system:

$$\begin{aligned} \mathcal{R}_{\xi, \psi}(\tau, \mathbf{z}) &= \sum_{t=0}^{T-1} \mathbf{r}_{\xi, \psi}(\mathbf{x}^t, \mathbf{a}^t, \mathbf{z}) \\ &= \sum_{t=0}^{T-1} \sum_{j=1}^N r_{\xi, \psi}(v_j^t, \mathbf{z}_j), \end{aligned}$$

with a joint policy denoted by  $\pi_\eta(\mathbf{a}^t|\mathbf{x}^t, \mathbf{z})$ . The cooperative assumption is not necessarily valid for generic traffic scenarios [17], but it simplifies the training procedure significantly. We will leave the extension of the proposed method to non-cooperative interactive traffic scenarios as a future work.

Given a demonstration dataset, we aim to infer the underlying reward function and policy. Different from a typical IRL problem, both  $r_{\xi, \psi}$  and  $\pi_\eta$  depend on  $\mathbf{z}$ . Therefore, we need to infer the distribution  $p(\mathbf{z}|\tau)$  to solve the IRL problem.

#### V. GROUNDED RELATIONAL INFERENCE

We now present the Grounded Relational Inference model to solve the IRL problem specified in Sec. IV. The model consists of three modules modeled by message-passing GNNs

[32]: an encoder inferring the posterior distribution of edge types, a policy decoder generates control actions conditioned on the edge variables sampled from the posterior distribution, and a reward decoder models the rewards conditioned on the inferred edge types.

### A. Architecture

The overall model structure is illustrated in Fig. 2. Given a demonstration trajectory  $\tau^E \in \mathcal{D}^E$ , the encoder operates over  $\mathcal{G}_{\text{scene}}$  and approximates the posterior distribution  $p(\mathbf{z}|\tau^E)$  with  $q_\phi(\mathbf{z}|\tau^E)$ . The policy decoder operates over a  $\mathcal{G}_{\text{interact}}$  sampled from the inferred  $q_\phi(\mathbf{z}|\tau^E)$  and models the policy  $\pi_\eta(\mathbf{a}^t|\mathbf{x}^t, \mathbf{z})$ . Given an initial state, we can generate a trajectory by sequentially sampling  $\mathbf{a}^t$  from  $\pi_\eta(\mathbf{a}^t|\mathbf{x}^t, \mathbf{z})$  and propagating the state. The state is propagated with either the transition operator  $\mathcal{T}$  if given, or a simulating environment if  $\mathcal{T}$  is not accessible. We denote a generated trajectory given the initial state of  $\tau^E$  as  $\tau^G$ . Since these two modules are essentially the same in NRI, we omit the detailed model structures here and include them in Appx. VIII-A.

The reward decoder computes the reward of a state-action pair given the sampled edge variables. We use it to compute the cumulative rewards of  $\tau^G$  and  $\tau^E$  conditioned on the sampled  $\mathcal{G}_{\text{interact}}$ . The reward decoder is in the form of Eqn. (4). Additionally, we augment the functions  $r_\xi^n$  and  $r_{\psi_k}^{e,k}$  with MLP shaping terms to mitigate the reward shaping effect [30], resulting in:

$$f_{\xi, \omega}^n(\mathbf{x}_j^t, \mathbf{a}_j^t, \mathbf{x}_j^{t+1}) = r_\xi^n(\mathbf{x}_j^t, \mathbf{a}_j^t) + h_\omega^n(\mathbf{x}_j^{t+1}) - h_\omega^n(\mathbf{x}_j^t),$$

and

$$\begin{aligned} f_{\psi_k, \chi_k}^{e,k}(\mathbf{x}_i^t, \mathbf{a}_i^t, \mathbf{x}_i^{t+1}, \mathbf{x}_j^t, \mathbf{a}_j^t, \mathbf{x}_j^{t+1}) &= r_{\psi_k}^{e,k}(\mathbf{x}_i^t, \mathbf{a}_i^t, \mathbf{x}_j^t, \mathbf{a}_j^t) \\ &+ h_{\chi_k}^{e,k}(\mathbf{x}_i^{t+1}, \mathbf{x}_j^{t+1}) - h_{\chi_k}^{e,k}(\mathbf{x}_i^t, \mathbf{x}_j^t), \end{aligned}$$

where  $h_\omega^n$  and  $h_{\chi_k}^{e,k}$  are MLPs with parameters denoted by  $\omega$  and  $\chi$  respectively. We denote the shaped reward function of agent  $v_j$  by  $\mathbf{f}_{\xi, \omega, \psi, \chi}(\mathbf{x}^t, \mathbf{a}^t, \mathbf{x}^{t+1}, \mathbf{z})$ , which equals to the left hand side of Eqn. (4) but with  $r_\xi^n$  and  $r_{\psi_k}^{e,k}$  substituted by the augmented rewards. The shaped reward function together with the policy model defines the discriminator which distinguishes  $\tau^G$  from  $\tau^E$ :

$$\begin{aligned} \mathcal{D}_{\xi, \omega, \psi, \chi, \eta}(\mathbf{x}^t, \mathbf{a}^t, \mathbf{x}^{t+1}, \mathbf{z}) \\ = \frac{\exp \{ \mathbf{f}_{\xi, \omega, \psi, \chi}(\mathbf{x}^t, \mathbf{a}^t, \mathbf{x}^{t+1}, \mathbf{z}) \}}{\exp \{ \mathbf{f}_{\xi, \omega, \psi, \chi}(\mathbf{x}^t, \mathbf{a}^t, \mathbf{x}^{t+1}, \mathbf{z}) \} + \pi_\eta(\mathbf{a}^t|\mathbf{x}^t, \mathbf{z})}. \end{aligned}$$

### B. Training

We aim to train the three modules simultaneously. Consequently, we incorporate the encoder model  $q_\phi(\mathbf{z}|\tau^E)$  into the objective function of AIRL, resulting in the optimization problem (6). The encoder is integrated into the minimization problem because the reward function has a direct dependence on the latent space. The model is then trained by solving problem (6) in an adversarial scheme: we alternate between training the encoder and reward for the minimization problem

and training the policy for the maximization problem. Specifically, the objective for the encoder and reward is the following minimization problem given fixed  $\eta$ :

$$\begin{aligned} \min_{\xi, \omega, \psi, \chi, \phi} \quad & \mathcal{J}(\xi, \omega, \psi, \chi, \phi, \eta) \\ \text{s.t.} \quad & \mathbb{E} \{ D_{KL} [q_\phi(\mathbf{z}|\tau^E))||p(\mathbf{z})] \} \leq I_c. \end{aligned} \quad (5)$$

The objective for the policy is maximizing  $\mathcal{J}(\xi, \omega, \psi, \chi, \phi, \eta)$  with fixed  $\xi, \omega, \psi, \chi$  and  $\phi$ .

The objective function in the problem (6) is essentially the expectation of the objective function in the problem (3) over the inferred posterior distribution  $q_\phi(\mathbf{z}|\tau^E)$  and the demonstration distribution  $\pi^E(\tau)$ . The constraint enforces an upper bound  $I_c$  on the KL-divergence between  $q_\phi(\mathbf{z}|\tau^E)$  and the prior distribution  $p(\mathbf{z})$ . A sparse prior is chosen to encourage sparsity in  $\mathcal{G}_{\text{interact}}$ . It has the similar regularization effect as the  $D_{KL}$  term in ELBO. We borrow its format from variational discriminator bottleneck (VDB) [22]. VDB improves adversarial training by constraining the information flow from the input to the discriminator. The KL-divergence constraint is derived as a variational approximation to the information bottleneck [33]. Although having different motivation, we adopt it for two reasons. First, the proposed model is not generative because our goal is not synthesizing trajectories from the prior  $p(\mathbf{z})$ , but inferring the posterior  $p(\mathbf{z}|\tau^E)$ . Therefore, regularization derived from information bottleneck is more sensible compared to ELBO. Second, the constrained problem (5) can be relaxed by introducing a Lagrange multiplier  $\beta$ . During training,  $\beta$  is updated through dual gradient descent as follows:

$$\beta \leftarrow \max (0, \alpha_\beta (\mathbb{E} \{ D_{KL} [q_\phi(\mathbf{z}|\tau^E))||p(\mathbf{z})] \} - I_c)) \quad (7)$$

We find the adaptation scheme particularly advantageous. The model can focus on inferring  $\mathbf{z}$  for reward learning after satisfying the sparsity constraint, because the magnitude of  $\beta$  decreases towards zero once the constraint is satisfied. However, it is worth noting that our framework does not rely on the bottleneck constraint to induce an interpretable latent space as in [34]. In contrast, GRI relies on the structured reward functions to ground the latent space into semantic interactive behaviors. The bottleneck serves as a regularization to find out the minimal interaction graph to represent the interactions. In fact, we trained the baseline NRI models with the same constraints and weight update scheme. The experimental results show that the constraint itself is not sufficient to induce a sparse and interpretable interaction graph.

In general, when the dynamics  $\mathcal{T}$  is unknown or non-differentiable, maximum entropy RL algorithms [35] are adopted to optimize the policy. In this work, we assume known and differentiable dynamics, which is a reasonable assumption for the investigated scenarios. It allows us to directly back-propagate through the trajectory for gradient estimation, which simplifies the training procedure.

## VI. EXPERIMENTS

We evaluated the proposed GRI model on a synthetic dataset as well as a naturalistic traffic dataset. The synthetic data were generated using policy models trained given the ground-truth

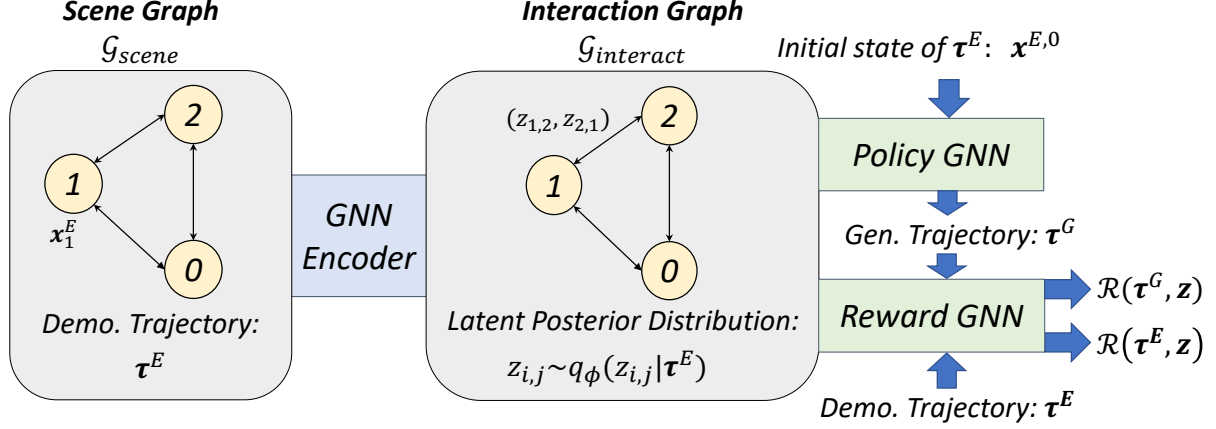


Fig. 2: Architecture of grounded interpretable relational inference model. Given a demonstration trajectory  $\tau^E \in \mathcal{D}^E$ , the encoder operates over  $\mathcal{G}_{\text{scene}}$  and approximates the distribution  $p(\mathbf{z}|\tau^E)$  with  $q_\phi(\mathbf{z}|\tau^E)$ . The policy decoder operates over a  $\mathcal{G}_{\text{interact}}$  sampled from the inferred  $q_\phi(\mathbf{z}|\tau^E)$  and models the policy  $\pi_\eta(\mathbf{a}^t|\mathbf{x}^t, \mathbf{z})$ . Given the initial state of  $\tau^E$ , we sample a trajectory  $\tau^G$  by sequentially sampling  $\mathbf{a}^t$  from  $\pi_\eta(\mathbf{a}^t|\mathbf{x}^t, \mathbf{z})$  and propagating the state. Finally, we use the reward GNN to compute the cumulative rewards of  $\tau^G$  and  $\tau^E$  conditioned on the sampled  $\mathcal{G}_{\text{interact}}$ .

$$\begin{aligned}
 \max_{\eta} \min_{\xi, \omega, \psi, \chi, \phi} \mathcal{J}(\xi, \omega, \psi, \chi, \phi, \eta) = & \mathbb{E}_{\tau^E \sim \pi^E(\tau)} \left\{ \mathbb{E}_{\mathbf{z} \sim q_\phi(\mathbf{z}|\tau^E)} \left[ - \sum_{t=0}^{T-1} \log \mathcal{D}_{\xi, \omega, \psi, \chi, \eta}(\mathbf{x}^{E,t}, \mathbf{a}^{E,t}, \mathbf{x}^{E,t+1}, \mathbf{z}) \right. \right. \\
 & \left. \left. - \mathbb{E}_{\tau^G \sim \pi_\eta(\tau|\mathbf{z})} \sum_{t=0}^{T-1} \log (1 - \mathcal{D}_{\xi, \omega, \psi, \chi, \eta}(\mathbf{x}^{G,t}, \mathbf{a}^{G,t}, \mathbf{x}^{G,t+1}, \mathbf{z})) \right] \right\}, \\
 \text{s.t. } & \mathbb{E}_{\tau^E \sim \pi^E(\tau)} \{ D_{KL} [q_\phi(\mathbf{z}|\tau^E) || p(\mathbf{z})] \} \leq I_c,
 \end{aligned} \tag{6}$$

reward function and interaction graph. We intend to verify if GRI can induce an interpretable relational latent space and infer the underlying relations precisely. The naturalistic traffic data were extracted from the NGSIM dataset. We aim to validate if GRI can model real-world traffic scenarios effectively with the grounded interpretable latent space. Unlike synthetic agents, we do not have the privilege to access the graphs governing human drivers' interactions. Instead, we constructed hypothetical graphs after analyzing the segmented data. The hypotheses reflect humans' understanding of the traffic scenarios. We would like to see if GRI can model real-world interactive systems in the same way as humans. We claim the model interpretable if the inferred interaction graphs are consistent with the hypotheses. In each setting, we consider two traffic scenarios, car-following (CF) and lane-changing (LC).

#### A. Baselines

The main question of interest is whether GRI can induce interpretable and semantic interaction graphs. To answer the question, the most important baseline model for comparison is NRI, because GRI shares the same prior distribution of latent variables with NRI. Comparing the posterior distributions provides insights on whether the structured reward functions can ground the latent space into semantic interactive behaviors. In each experiment, the baseline NRI model has the same encoder and policy decoder as the GRI model. Besides, as

stated in Sec. V, the same bottleneck constraint and the weight update scheme in Eqn. (7) were applied as regularization for minimal representation.

Another model for comparison is a supervised policy decoder. We assume that the ground-truth graphs or human hypotheses are available. Therefore, we can directly train a policy decoder in a supervised way. The ground-truth graph is fed to the policy decoder as a substitute for the interaction graph sampled from the encoder output  $q_\phi(\mathbf{z}|\tau^E)$ . The training of the decoder becomes a regression problem. We used mean square error as the loss function to train it.

As additional information is granted, it is unfair to directly compare the performance of GRI with the supervised policy model. However, the supervised baseline provides some useful insights. Since the supervised model is trained with the ground-truth interaction graphs governing the systems, it is expected to achieve smaller reconstruction error. However, as we argue in Sec. I, even if interaction labels are available, the supervised model is not guaranteed to understand the semantic meaning behind the labels and synthesize the right behaviors. We demonstrate the advantage of GRI over both baselines on this problem in some simple out-of-distribution experiments. The details are discussed in Sec. VI-E. Additionally, in the naturalistic traffic scenarios, the supervised model gives us some insights on whether the human hypotheses are reasonable. If the supervised model can reconstruct the trajectories precisely, it will justify our practice to adopt graph accuracy as one of

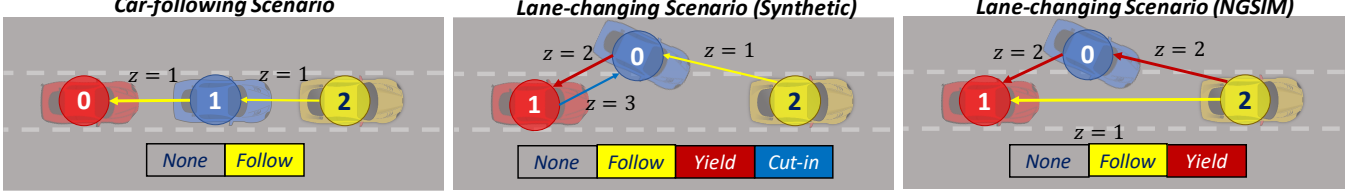


Fig. 3: Test scenarios with the underlying interaction graphs. In the synthetic scenarios, the graphs are the ground-truth ones governing the synthetic experts. In the naturalistic traffic scenarios, the graphs are human hypotheses reflecting humans' understanding of the traffic scenarios.

the evaluation metrics.

There exist other alternatives for the purpose of trajectory reconstruction. However, it is not our goal in this paper to find an expressive model for accurate reconstruction. Therefore, we do not consider other baselines from this perspective. For the task of grounding the latent space into semantic interactive driving behaviors, we did not find any exact alternatives in the literature. There could exist some heuristics or rule-based approaches to directly determine an interpretable interaction graph, especially for the specific scenarios studies in this paper. However, they are not within the scope of discussion for this paper because we are interested in a data-driven framework that can be integrated into a learning-based autonomous driving model, and has the potential to be generalized to complicated driving scenarios and systems in other domains.

### B. Evaluation Metrics

To evaluate a trained model, we sample a  $\tau^E$  from the test dataset and extract the maximum posterior probability (MAP) estimate of edge variables,  $\hat{\mathbf{z}}$ , from  $q_\phi(\mathbf{z}|\tau^E)$ . Afterward, we obtain a single sample of trajectories  $\hat{\tau}$  by executing the mean value of the policy output. The root mean square errors (RMSE) of states and the accuracy of  $\mathcal{G}_{\text{interact}}$  are selected as the evaluation metrics, which are computed based on  $\hat{\mathbf{z}}$ ,  $\hat{\tau}$ ,  $\tau^E$ , and the ground truth or hypothetical latent variables denoted by  $\mathbf{z}^E$ :

$$\text{RMSE}_\epsilon = \sqrt{\frac{1}{(N-1)T} \sum_{j=1}^N \sum_{t=0}^{T-1} (\epsilon_j^{E,t} - \hat{\epsilon}_j^t)^2},$$

$$\text{Accuracy} = \frac{\sum_{i=1}^N \sum_{j=1, j \neq i}^N \mathbf{1}(z_{i,j}^E = \hat{z}_{i,j})}{N(N-1)}.$$

If multiple edge types exist, we test all the possible permutations of edge types and report the one with the highest graph accuracy for NRI.

### C. Synthetic Scenes

As mentioned above, we designed two synthetic scenarios, car-following and lane-changing. The two scenes and their underlying interaction graphs are illustrated in Fig. 3. In both scenarios, we have a leading vehicle whose behavior does not depend on the others. Its trajectory is given without the need of reconstruction. We simply assume it runs at constant velocity. The other vehicles interact with each other and the leading

one in different ways. In CF, we model the system with two types of edges:  $z_{i,j} = 1$  means that Vehicle  $j$  follows Vehicle  $i$ ;  $z_{i,j} = 0$  means that Vehicle  $j$  does not interact with Vehicle  $i$ . In LC, two additional edge types are introduced:  $z_{i,j} = 2$  means that Vehicle  $j$  yields to Vehicle  $i$ ;  $z_{i,j} = 3$  means that Vehicle  $j$  cuts in front of Vehicle  $i$ .

The MDPs for the tested scenarios are specified as follows. In CF, since the vehicles mainly interact in longitudinal direction, we only model their longitudinal dynamics to simplify the problem. For all  $j \in \{1, 2, 3\}$ , the state vector of Vehicle  $j$  consists of three states:  $\mathbf{x}_j^t = [x_j^t \ v_j^t \ a_j^t]^\top$ , where  $x_j^t$  is the longitudinal coordinate,  $v_j^t$  is the velocity, and  $a_j^t$  is the acceleration. There is only one control input which is the jerk. We denote it as  $\delta a_j^t$ . The dynamics is governed by a 1D point-mass model:

$$x_j^{t+1} = x_j^t + v_j^t \Delta t + \frac{1}{2} a_j^t \Delta t^2,$$

$$v_j^{t+1} = v_j^t + a_j^t \Delta t,$$

$$a_j^{t+1} = a_j^t + \delta a_j^t \Delta t,$$

where  $\Delta t$  is the sampling time. In LC, we consider both longitudinal and lateral motions. The state vector consists of six states instead:  $\mathbf{x}_j^t = [x_j^t \ y_j^t \ v_j^t \ \theta_j^t \ a_j^t \ \omega_j^t]^\top$ . The three additional states are the lateral coordinate  $y_j^t$ , the yaw angle  $\theta_j^t$ , and the yaw rate  $\omega_j^t$ . There is one additional action which is the yaw acceleration, denoted by  $\delta \omega_j^t$ . We model the vehicle as a Dubins' car:

$$x_j^{t+1} = x_j^t + v_j^t \cos(\theta_j^t) \Delta t,$$

$$y_j^{t+1} = y_j^t + v_j^t \sin(\theta_j^t) \Delta t,$$

$$v_j^{t+1} = v_j^t + a_j^t \Delta t,$$

$$\theta_j^{t+1} = \theta_j^t + \omega_j^t \Delta t,$$

$$a_j^{t+1} = a_j^t + \delta a_j^t \Delta t,$$

$$\omega_j^{t+1} = \omega_j^t + \delta \omega_j^t \Delta t.$$

The structured reward functions were designed based on expert domain knowledge (e.g. transportation studies [31], [36]). We mainly referred to [13] in this paper. For the car-following behavior, its reward function is defined as follows:

$$r_{\psi_1}^{e,1}(\mathbf{x}_i^t, \mathbf{x}_j^t) = -(1 + \exp(\psi_{1,0})) g_{\text{IDM}}(\mathbf{x}_i^t, \mathbf{x}_j^t) - (1 + \exp(\psi_{1,1})) g_{\text{dist}}(\mathbf{x}_i^t, \mathbf{x}_j^t) - (1 + \exp(\psi_{1,2})) g_{\text{lat}}(\mathbf{x}_i^t, \mathbf{x}_j^t),$$

TABLE I: Performance Comparison on Synthetic Dataset

Model	Car Following ( $\Delta t = 0.2s, T = 20$ )			Lane Changing ( $\Delta t = 0.2s, T = 30$ )			
	RMSE <sub>x</sub> (m)	RMSE <sub>v</sub> (m/s)	Accuracy(%)	RMSE <sub>x</sub> (m)	RMSE <sub>y</sub> (m)	RMSE <sub>v</sub> (m/s)	Accuracy(%)
GRI	$0.241 \pm 0.125$	$0.174 \pm 0.068$	<b><math>100.00 \pm 0.00</math></b>	$0.636 \pm 0.297$	$0.273 \pm 0.060$	$0.344 \pm 0.135$	<b><math>99.95 \pm 0.01</math></b>
NRI	$0.047 \pm 0.024$	$0.056 \pm 0.015$	$66.70 \pm 0.00$	$0.116 \pm 0.046$	$0.197 \pm 0.049$	$0.084 \pm 0.022$	$66.70 \pm 0.00$
Supervised	<b><math>0.039 \pm 0.016</math></b>	<b><math>0.050 \pm 0.009</math></b>	-	<b><math>0.114 \pm 0.041</math></b>	<b><math>0.174 \pm 0.045</math></b>	<b><math>0.063 \pm 0.014</math></b>	-

<sup>1</sup> The data is presented in form of mean  $\pm$  std.

where the features are defined as:

$$g_{\text{IDM}}(\mathbf{x}_i^t, \mathbf{x}_j^t) = \left( \max(x_i^t - x_j^t, 0) - \Delta x_{i,j}^{\text{IDM},t} \right)^2, \quad (8)$$

$$g_{\text{dist}}(\mathbf{x}_i^t, \mathbf{x}_j^t) = \exp \left( - \frac{(\max(x_i^t - x_j^t, 0))^2}{\zeta^2} \right), \quad (9)$$

$$g_{\text{lat}}(\mathbf{x}_i^t, \mathbf{x}_j^t) = (y_j^t - g_{\text{center}}(y_i^t))^2.$$

The feature  $g_{\text{IDM}}$  suggests a spatial headway  $\Delta x_{i,j}^{\text{IDM},t}$  derived from the intelligent driver model (IDM) [31]. The feature  $f_{\text{dist}}$  ensures a minimum collision-free distance. We penalize the following vehicle for surpassing the preceding one with the help of  $x_{i,j}^{\text{IDM},t}$  in Eqn. (8) and Eqn. (9). The last feature  $g_{\text{lat}}$  exists only in LC. It regulates the following vehicle to stay in the same lane as the preceding one with the help of  $g_{\text{center}}$ , which determines the lateral coordinate of the corresponding centerline based on the position of the preceding vehicle.

The reward function for yielding is defined as:

$$r_{\psi_2}^{e,2}(\mathbf{x}_i^t, \mathbf{x}_j^t) = -(1 + \exp(\psi_{2,0})) g_{\text{yield}}(\mathbf{x}_i^t, \mathbf{x}_j^t) - (1 + \exp(\psi_{2,1})) g_{\text{dist}}(\mathbf{x}_i^t, \mathbf{x}_j^t).$$

The feature  $g_{\text{dist}}$  is defined in Eqn. (9). The other feature  $g_{\text{yield}}$  suggests an appropriate spatial headway for yielding:

$$g_{\text{yield}}(\mathbf{x}_i^t, \mathbf{x}_j^t) = \mathbf{1}(g_{\text{center}}(y_j^t) = g_{\text{center}}(y_i^t)) g_{\text{IDM}}(\mathbf{x}_i^t, \mathbf{x}_j^t) + \mathbf{1}(g_{\text{center}}(y_j^t) \neq g_{\text{center}}(y_i^t)) g_{\text{goal}}(\mathbf{x}_i^t, \mathbf{x}_j^t),$$

$$g_{\text{goal}}(\mathbf{x}_i^t, \mathbf{x}_j^t) = (\max(x_i^t - x_j^t - \Delta x^{\text{yield}}, 0))^2. \quad (10)$$

The suggested headway is set to be a constant value,  $\Delta x^{\text{yield}}$ , when the other vehicle is merging, and switches to  $\Delta x_{i,j}^{\text{IDM},t}$  once the merging vehicle enters into the same lane, where its behavior becomes consistent with car following.

The reward function for cutting-in is quite similar:

$$r_{\psi_3}^{e,3}(\mathbf{x}_i^t, \mathbf{x}_j^t) = -(1 + \exp(\psi_{3,0})) g_{\text{goal}}(\mathbf{x}_i^t, \mathbf{x}_j^t) - (1 + \exp(\psi_{3,1})) g_{\text{dist}}(\mathbf{x}_j^t, \mathbf{x}_i^t),$$

where the features are defined as in Eqn. (9) and Eqn. (10), but with the input arguments switched, because the merging vehicle should stay in front of the yielding one.

Apart from the edge rewards, all the agents share the same node reward function. The following one is adopted for LC:

$$r_{\xi}^n(\mathbf{x}_j^t, \mathbf{a}_j^t) = -(1 + \exp(\xi_0)) f_v(\mathbf{x}_j^t) - (1 + \exp(\xi_{1:3}))^T f_{\text{state}}(\mathbf{x}_j^t) - (1 + \exp(\xi_{4:5}))^T f_{\text{action}}(\mathbf{a}_j^t) - (1 + \exp(\xi_6)) f_{\text{lane}}(\mathbf{x}_j^t),$$

where  $f_{\text{state}}$  and  $f_{\text{action}}$  take the element-wise square of  $[a_j^t \theta_j^t \omega_j^t]$  and  $[\delta a_j^t \delta \omega_j^t]$  respectively. The feature  $f_v$  is the squared error between  $v_j^t$  and the speed limit  $v_{\text{lim}}$ . The last

term  $f_{\text{lane}}$  penalizes the vehicle for staying close to the lane boundaries. For CF, we simply remove those terms that are irrelevant in 1D motion. In all the reward functions, the parameters collected in  $\psi$  and  $\xi$  are unknown during training and inferred by GRI. We take the exponents of them and add one to the results. It enforces the model to use the features when modeling the corresponding interactions.

With the scenarios defined above, we aim to generate one dataset for each scenario. For each scenario, we randomly sampled the initial states of the vehicles and trained an expert policy given the ground-truth reward functions and the interaction graph. Afterwards, we used the trained policy to generate the dataset. The same sampling scheme was used to sample the initial states.

**Results.** On each dataset, we trained a GRI model with the policy decoder (16)-(18) introduced in Appx. VIII-A. The results are summarized in Table I. The NRI model can reconstruct the trajectories with errors close to the supervised policy. However, it learns a relational latent space that is different from the one underlying the demonstration; Therefore, the edge variables cannot be interpreted as those semantically meaningful behaviors. In contrast, our GRI model interprets the interactions consistently with the domain knowledge inherited in the demonstration, and recovers the interaction graph with high accuracies.

To further evaluate the explainability of the inferred graphs, we computed the empirical distribution of the estimated edge variables  $\hat{z}$  over the test dataset. The results are summarized in Fig. 4. It shows the empirical distribution in multiple adjacency matrices corresponding to different edge types. The distribution concentrates into a single interaction graph for both models in both scenarios—as opposed to the case on the naturalistic traffic dataset which will be introduced in the next section—because the synthetic agents have consistent interaction patterns over all the samples. In CF, the interaction graph of the NRI model has two additional edges compared to the ground-truth one:  $z_{2,0} = 1$  and  $z_{0,1} = 1$ . It is fairly reasonable to have  $z_{2,0} = 1$  because Vehicle 2 affects Vehicle 0 in an indirect way. On the other hand,  $z_{0,1} = 1$  is not consistent with the inherent causality and cannot be interpreted as car-following as the other edges. In LC, the NRI model treats the edges  $e_{1,0}$ ,  $e_{0,1}$ , and  $e_{2,1}$  the same, which makes it difficult to interpret the semantic meaning behind, because these edges correspond to distinct interactive behaviors in the expert demonstration.

#### D. Naturalistic Traffic Scenes

To evaluate the proposed method in real-world traffic scenarios, we investigated the same scenarios as in the synthetic

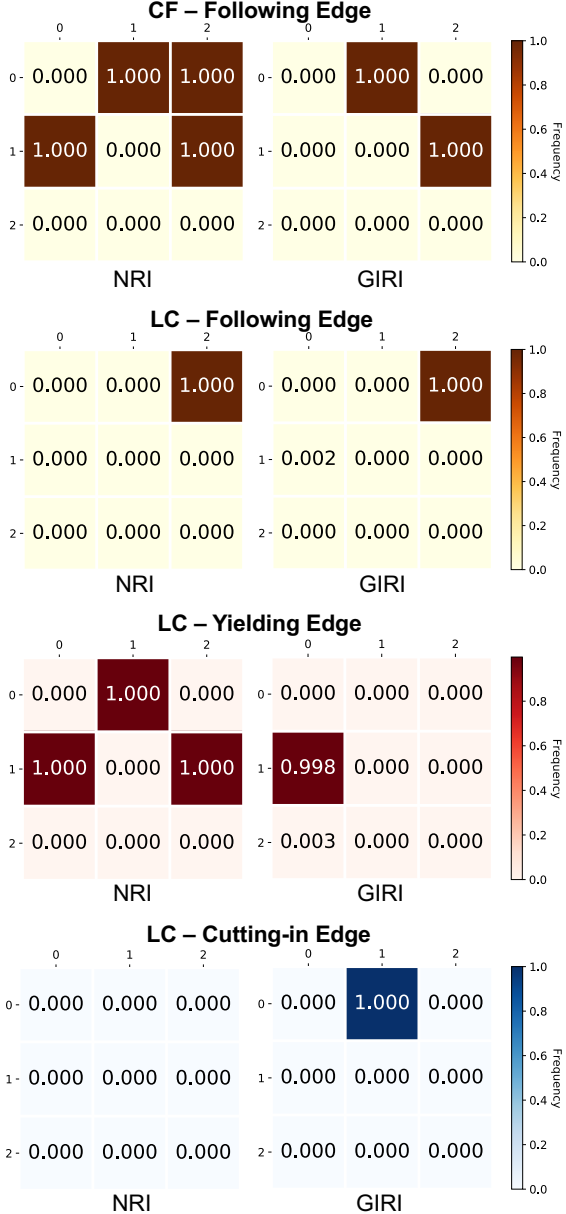


Fig. 4: The empirical distribution of estimated edge variables  $\hat{z}$  over the test dataset in the synthetic scenarios. We summarize the results in multiple adjacency matrices corresponding to different edge types. In the adjacency matrix corresponding to the  $k^{\text{th}}$  type of interaction, the element  $A_{i,j}$  indicates the relative frequency of  $z_{j,i} = k$ , where  $z_{j,i}$  is the latent variable for the edge from node  $j$  to node  $i$ .

case, car-following and lane-changing. we segmented data from the Highway-101 and I-80 datasets of NGSIM. Afterwards, we further screened the data to select those interactive samples and ensure that no erratic swerving or multiple lane changes occur. Unlike the synthetic agents, human agents do not have a ground-truth interaction graph that governs their interactions. Instead, we constructed hypothetical  $\mathcal{G}_{\text{interact}}$  after analyzing the segmented data. The hypotheses reflect humans' understanding of the traffic scenarios. We would like

to see if GRI can model the real-world interactive systems in a consistent way as humans. The hypotheses for the two scenarios are depicted in Fig. 3. The one for CF is identical to the ground-truth interaction graph we designed for the synthetic agents. However, we proposed a different hypothesis for LC. We excluded the cutting-in relation to reduce the number of edge types and therefore simplify the training procedure. Moreover, we differentiated distinct interactions according to the vehicles' lateral position. We say that a vehicle yields to its preceding vehicle if they drive in neighbouring lanes, whereas it follows the preceding one if they drive in the same lane.

The node dynamics is the same as in the synthetic scene for CF. For LC, since we did not have accurate heading information, we adopted 2D point-mass model instead. Since the behavior of human drivers is much more complicated than the synthetic agents, we designed reward functions with larger model capacity using neural networks. In CF, the reward functions are defined as follows:

$$\begin{aligned} r_{\psi_1}^{e,1}(\mathbf{x}_i^t, \mathbf{x}_j^t) &= -(1 + \exp(\psi_{1,0})) g_v^{\text{NN}}(\mathbf{x}_i^t, \mathbf{x}_j^t) \\ &\quad -(1 + \exp(\psi_{1,1})) g_s^{\text{NN}}(\mathbf{x}_i^t, \mathbf{x}_j^t), \\ r_{\xi}^n(\mathbf{x}_j^t, \mathbf{a}_j^t) &= -(1 + \exp(\xi_0)) f_v^{\text{NN}}(\mathbf{x}_j^t) \\ &\quad -(1 + \exp(\xi_1)) f_{\text{acc}}(\mathbf{x}_j^t) \\ &\quad -(1 + \exp(\xi_2)) f_{\text{jerk}}(\mathbf{x}_j^t, \mathbf{a}_j^t), \end{aligned}$$

where the features are defined as:

$$\begin{aligned} f_v^{\text{NN}}(\mathbf{x}_j^t) &= (v_j^t - h_1(\mathbf{x}_j^t))^2, \\ g_v^{\text{NN}}(\mathbf{x}_i^t, \mathbf{x}_j^t) &= (v_j^t - h_2(\mathbf{x}_i^t, \mathbf{x}_j^t))^2, \\ g_s^{\text{NN}}(\mathbf{x}_i^t, \mathbf{x}_j^t) &= \text{ReLU}(h_3(\mathbf{x}_i^t, \mathbf{x}_j^t) - x_i^t + x_j^t)^2. \end{aligned}$$

The features  $f_{\text{acc}}$  and  $f_{\text{jerk}}$  penalize the squared magnitude of acceleration and jerk. The functions  $h_1$ ,  $h_2$  and  $h_3$  are neural networks with ReLU output activation. The feature  $g_s^{\text{NN}}$  is the critical component which shapes the car-following behavior. It learns a non-negative reference headway and penalizes the following vehicle for violating it. The feature  $g_v^{\text{NN}}$  and  $f_v^{\text{NN}}$  suggest reference velocities considering interaction and merely itself respectively.

In LC, the edge reward function for car-following and the node reward function are similar to those in CF, with additional terms for lateral position, velocity and acceleration. Particularly, the node reward for lateral position encourages the vehicles to drive on the target lane, i.e., the lane where the leading vehicle is driving. To design the yielding reward, we define a collision point of two vehicles based on their states. We approximate the vehicles' trajectories as piecewise-linear between sequential timesteps, and compute the collision point as the intersection between their trajectories (Fig. 5). We threshold the point if it exceeds a hard-coded range of interest (e.g. if it is behind the vehicles or greater than certain distance). Afterwards, we define the distance-to-collision ( $d_{\text{poc}}$ ) as the longitudinal distance from the vehicle to the collision point, and the time-to-collision ( $T_{\text{col}}$ ) as the time to reach the collision point calculated by dividing  $d_{\text{poc}}$  with the velocity

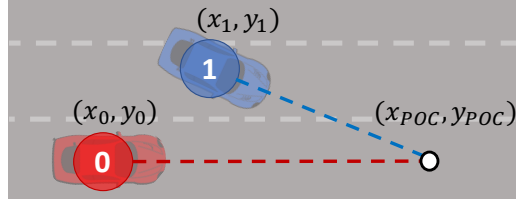


Fig. 5: Collision point diagram. At every timestep, the heading vector of the agents' can be calculated approximating the motion as linear. The intersection between these vectors is taken to be the collision point where the agents would collide if a yield action is not taken.

of the vehicle. Then the yielding reward function is defined as follows:

$$r_{\psi_2}^{e,2}(\mathbf{x}_i^t, \mathbf{x}_j^t) = -(1 + \exp(\psi_{2,0})) g_{\text{spatial}}^{\text{NN}}(\mathbf{x}_i^t, \mathbf{x}_j^t) - (1 + \exp(\psi_{2,1})) g_{\text{time}}^{\text{NN}}(\mathbf{x}_i^t, \mathbf{x}_j^t),$$

where

$$g_{\text{spatial}}^{\text{NN}}(\mathbf{x}_i^t, \mathbf{x}_j^t) = \text{ReLU}((x_j - x_{poc}) - h_{d_{poc}}(\mathbf{x}_i^t, \mathbf{x}_j^t))^2, \\ g_{\text{time}}^{\text{NN}}(\mathbf{x}_i^t, \mathbf{x}_j^t) = \text{ReLU}(h_{T_{\text{col}}}(\mathbf{x}_i^t, \mathbf{x}_j^t) - (T_{\text{col}_i} - T_{\text{col}_j}))^2.$$

The functions  $h_{d_{poc}}$  and  $h_{T_{\text{col}}}$  are neural networks with ReLU output activation. The  $g_{\text{spatial}}$  term learns a spatial aspect of the yield behavior and compares the agent's distance from the estimated collision-point with the NN-learned *safe* reference within which the LC maneuver can be done. The second term  $g_{\text{time}}$  adds a temporal aspect to yield and compares a learned *safe* headway time and to the difference in time-to-collision for the two vehicles. The intuition behind is to ensure that the vehicles do not occupy the same position at the same time.

**Results.** For each scenario, we trained a GRI model with the recurrent policy decoder (19)-(22) in Appx. VIII-A. The results are summarized in Table II. In CF, the NRI model still performs better on trajectory reconstruction, but the GRI model achieves comparable RMSE on NGSIM dataset. Moreover, we observed that the NRI model overfitted to the training dataset, whereas the GRI model performs consistently on both training and test datasets. It shows that incorporating domain knowledge in a principled manner is an effective regulation to avoid overfitting. In LC, their comparison is consistent: The NRI model slightly outperforms our model in trajectory reconstruction; Our model dominates the NRI model in graph accuracy. For the supervised policy, it has the lowest reconstruction error in LC. And its performance in CF is comparable to the NRI model. It implies that the human hypotheses are reasonable assumptions which are capable to model the interactions between human drivers.

We visualize the interaction graphs in Fig. 6. One interesting observation is that the graphs inferred by NRI have more edges in general. We want to emphasize that both models are trained under the same sparsity constraint. The results imply that we could guide the model to explore a clean and sparse representation of interactions by incorporating relevant domain knowledge, whereas the sparsity regularization itself is not sufficient to serve the purpose. Moreover, the NRI model

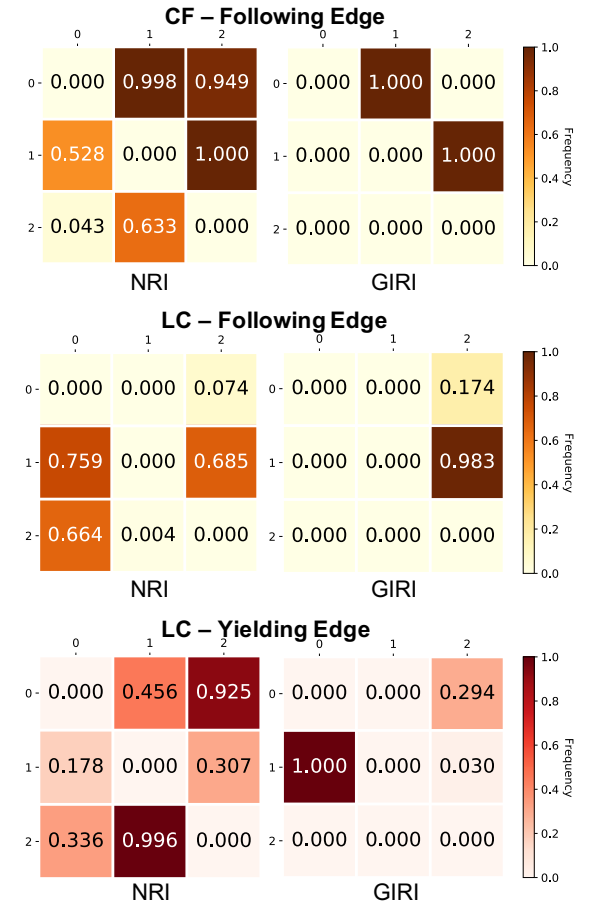


Fig. 6: The empirical distribution of estimated edge variables  $\hat{z}$  over the test dataset in the naturalistic traffic scenarios. We summarize the results in multiple adjacency matrices corresponding to different edge types. In the adjacency matrix corresponding to the  $k^{\text{th}}$  type of interaction, the element  $A_{i,j}$  indicates the relative frequency of  $z_{j,i} = k$ , where  $z_{j,i}$  is the latent variable for the edge from node  $j$  to node  $i$ .

assigns the same edge type to both edges between a pair of agents. It makes the graphs less interpretable because the vehicles ought to affect each other in different ways. On the other hand, even if different from the hypotheses, our GRI model tends to infer sparse graphs with directional edges.

### E. Out-of-distribution Experiments

Because of the smaller reconstruction errors, it appears that the NRI model discovers a relational latent space that can effectively model the interactions, which makes it a more favorable option. The interpretability of the inferred graphs seems less important when the reconstruction is substantially accurate. However, we would like to emphasize that a semantically meaningful latent space that is consistent with humans' prior knowledge is necessary, especially if we want to deploy the models in real-world settings for applications in human-robot interaction. We demonstrate it with the following out-

TABLE II: Performance Comparison on Naturalistic Traffic Dataset

Model	Car Following ( $\Delta t = 0.2s, T = 30$ )			Lane Changing ( $\Delta t = 0.2s, T = 40$ )			
	RMSE <sub>x</sub> (m)	RMSE <sub>y</sub> (m/s)	Accuracy(%)	RMSE <sub>x</sub> (m)	RMSE <sub>y</sub> (m)	RMSE <sub>v</sub> (m/s)	Accuracy(%)
GRI	$1.700 \pm 1.005$	$0.721 \pm 0.363$	<b><math>100.00 \pm 0.00</math></b>	$7.118 \pm 3.647$	$0.764 \pm 0.336$	$4.320 \pm 2.392$	<b><math>98.55 \pm 0.06</math></b>
NRI	<b><math>1.436 \pm 0.880</math></b>	<b><math>0.650 \pm 0.328</math></b>	$64.09 \pm 0.08$	$6.532 \pm 3.822$	$0.330 \pm 0.181$	<b><math>4.291 \pm 2.544</math></b>	$28.98 \pm 0.08$
Supervised	$1.482 \pm 0.938$	$0.665 \pm 0.344$	-	<b><math>5.897 \pm 3.651</math></b>	<b><math>0.323 \pm 0.223</math></b>	$4.307 \pm 2.435$	-

<sup>1</sup> The data is presented in form of mean  $\pm$  std.

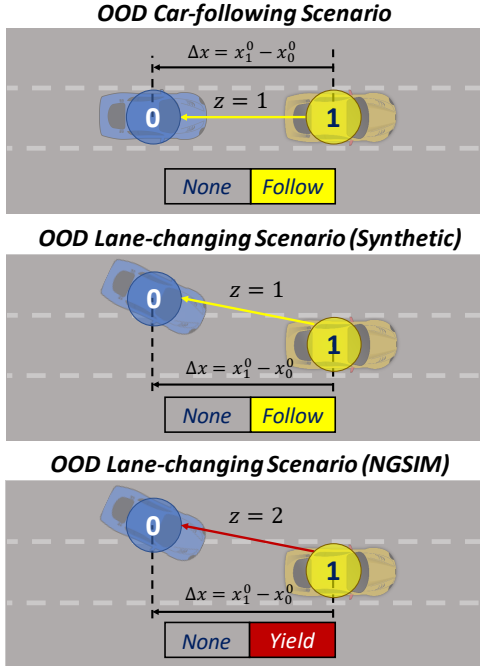


Fig. 7: Out-of-distribution scenarios. We removed one vehicle from the nominal scenes and shifted the initial longitudinal headway  $\Delta x$  to unseen values.

of-distribution tests<sup>2</sup>.

For the synthetic scenarios, we removed one vehicle from each scene: Vehicle 0 in CF and Vehicle 1 in LC, resulting in two interaction graphs consisting merely of following relations (Fig. 7). Also, we decreased the initial longitudinal headway to values unseen during the training stage. The initial longitudinal headway is defined as  $\Delta x = x_1^0 - x_0^0$ , namely the longitudinal distance from Vehicle 1 to Vehicle 0 at the first time step. During the training stage, we sampled  $\Delta x$  from uniform distributions: In CF,  $\Delta x \sim \text{unif}(4, 8)$ ; In LC,  $\Delta x \sim \text{unif}(8, 12)$ . In the out-of-distribution experiments, we gradually decreased  $\Delta x$  from the lower bound to some negative value, which means Vehicle 0 is placed in front of Vehicle 1.

Instead of evaluating the entire model, we enforced the ground-truth  $\mathcal{G}_{\text{interact}}$ <sup>3</sup>, and ran the policy decoders to generate trajectories. The experiment is analogous to the case when the vehicle encounters an unfamiliar situation. The safety drivers or passengers have the privilege to override the inferred graph

<sup>2</sup>For clarification, the models used in this section are the same as those introduced in Sec. VI-C. We merely designed additional out-of-distribution cases for testing.

<sup>3</sup>For the NRI model, since the edge types are not defined explicitly, we use the permutation found with the highest graph accuracy to find out the corresponding edge type, when multiple edge types exist.

to let the desired behavior emerge if the model misunderstands the scenario. Such kind of safety assurance could help building up a safe and trustworthy cooperation between humans and the autonomous vehicles. It is then crucial that the latent space possesses explicit semantic meanings and corresponds to a cluster of semantically meaningful interactive behaviors. Therefore, we are curious about if the models can generate trajectories meeting the characteristics of the car-following behavior in these unseen scenarios—scenarios with a different number of vehicles and distorted state distribution. We consider three metrics for quantitative evaluation:

- Final headway:

$$\Delta x^f = x_1^T - x_0^T, \quad (11)$$

- Lateral distance:

$$\Delta y = |y_1^T - y_0^T| - |y_1^0 - y_0^0|, \quad (12)$$

- Minimum distance:

$$d_{\min} = \min_i \sqrt{|x_1^i - x_0^i|^2 + |y_1^i - y_0^i|^2}. \quad (13)$$

We intend to quantify three typical characteristics of the following behavior with the metrics defined above: 1) staying behind the leading vehicle; 2) keeping in the same lane as the leading vehicle; 3) maintaining a substantial safe distance from the leading vehicle. All metrics were applied in LC, but we only adopted the final headway in CF. Since only the longitudinal dynamics is modeled in CF,  $\Delta y$  is not applicable. For the same reason, if their initial positions are too close or the following vehicle located ahead of the leading one initially, the following vehicle will inevitably crush into the leading vehicle, which results in  $d_{\min} = 0$ . Therefore, we only care about the first characteristic and its corresponding metric.

The results are summarized in Fig. 8 and Fig. 9, where we plot the mean values of the evaluated metrics versus  $\Delta x$ , with error bands denoting 95% confidence interval. We are particularly interested in the cases when  $\Delta x$  becomes negative, which changes the spatial relations between the vehicles.

In CF, the NRI policy does not slow down Vehicle 0 to follow Vehicle 1 when  $\Delta x$  becomes negative, resulting in negative  $\Delta x^f$ . In contrast, the supervised policy and GRI policy maintain a positive average  $\Delta x^f$ , which means they yield Vehicle 0 to follow Vehicle 1. However, the GRI policy attains a larger  $\Delta y^f$  and the margin becomes larger with decreasing  $\Delta y$ . We visualize a marginal example in Fig. 12, where both the NRI policy and the supervised one fail to maintain a positive final headway.

In LC, the pattern of the final headway is the same. The GRI policy maintains a consistent  $\Delta x^f$  over all tested values of  $\Delta x$ . For the other two models, the values of  $\Delta x^f$  decrease

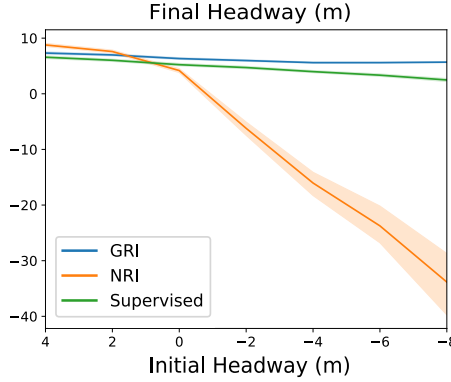


Fig. 8: Results in out-of-distribution synthetic car-following scenario. We plot the mean values of  $\Delta x^f$  versus  $\Delta x$  with error bands denoting 95% confidence interval. A positive headway means that Vehicle 0 stays behind Vehicle 1, whereas a negative headway means that Vehicle 0 locates in front of Vehicle 1.

with decreasing  $\Delta x$ . The average  $\Delta x^f$  of the NRI policy turns negative when the magnitude of  $\Delta x$  becomes sufficiently large. In terms of  $\Delta y$ , all models tend to reduce the lateral distance between the vehicles which is consistent with the second characteristic of the following behavior. However, we found that the GRI policy attains an average  $\Delta y$  with smaller magnitude and the magnitude decreases with decreasing  $\Delta x$ . It implies that the GRI policy changes its strategy when the initial position of Vehicle 0 is ahead of Vehicle 1. In order to keep a proper safe distance, Vehicle 0 does not change its lane until Vehicle 1 surpasses itself. On the other hand, the lateral behavior is unchanged for the other two models. However, the vehicle cannot maintain a substantial safe distance if it changes its lane too early, which is verified by the plot of  $d_{\min}$  versus  $\Delta x$ . The difference in their strategies is further demonstrated by the example visualized in Fig. 12.

We repeated the experiment on the NGSIM datasets. Similar to the case of synthetic dataset, we removed one vehicle from each scene, resulting in interaction graphs consisting of a single edge (Fig. 7). The only difference is that the remaining edge in LC is of yielding type. However, according to our definition of yielding relation, we considered the same characteristics and adopted the same metrics defined in Eqn. (11)-(13) for evaluation. Since we do not have control over the data generation procedure, we generate out-of-distribution test samples with different levels of discrepancy by controlling the ratio of longitudinal headway change. Given a sample from the original test dataset, we generate its corresponding out-of-distribution sample by shifting its initial longitudinal headway  $\Delta x$  by a certain ratio, denoted by  $\delta$ , resulting in a new value of longitudinal headway  $\Delta x'$ :

$$\Delta x' = (1 - \delta)\Delta x.$$

We evaluated the models on datasets generated with different values of  $\delta$ . We are particularly interested in the cases when  $\delta \geq 1$ , which leads to a negative initial headway. We present the results in Fig. 10 and 11, where we plot the mean

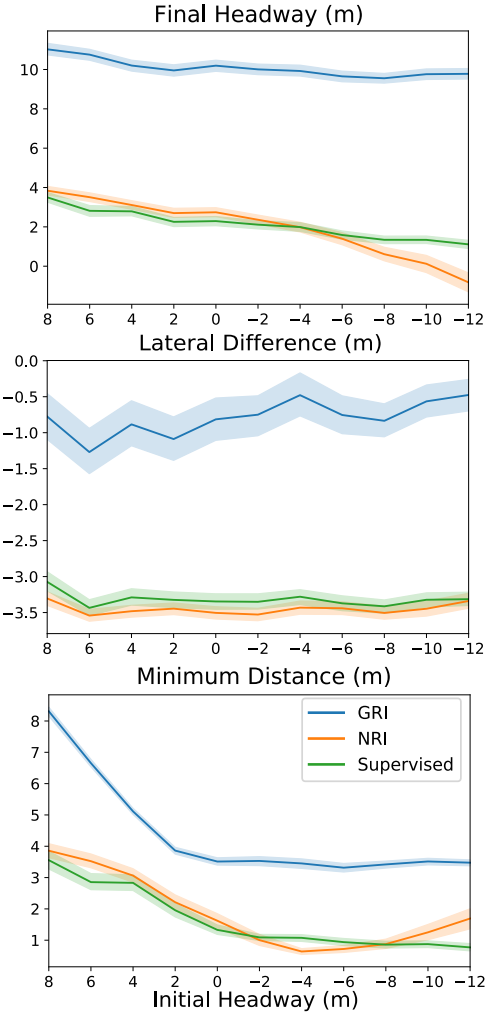


Fig. 9: Results in out-of-distribution synthetic lane-changing scenario. We plot the mean values of  $\Delta x^f$ ,  $\Delta y$ , and  $d_{\min}$  versus  $\Delta x$  with error bands denoting 95% confidence interval. A positive headway means that Vehicle 0 stays behind Vehicle 1, whereas a negative headway means that Vehicle 0 locates in front of Vehicle 1. A negative lateral difference means that Vehicle 0 is getting to the same lane as Vehicle 1. A minimum distance close to zero means that the vehicles collide to each other at least once during the tested time horizon.

values of the metrics versus  $\delta$ , with error bands denoting 95% confidence interval. The comparison is quite consistent with the synthetic scenarios. Compared to the other baselines, our GRI policy can synthesize trajectories that satisfy the desired semantic properties in a larger range of distribution shift.

The results suggest that even though the NRI model can accurately reconstruct the trajectories, the unsupervised latent space does not necessarily model the underlying interactions precisely. The latent space and the corresponding policies do not capture the semantic meanings behind the interactions. As a result, the model is prone to failure at unseen scenarios. And the non-interpretable nature prohibits effective human intervention in these circumstances. In contrast, the semantically meaningful latent space and policy of GRI enable safe

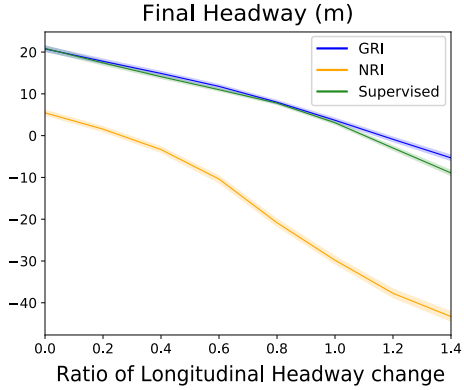


Fig. 10: Results in out-of-distribution naturalistic traffic car-following scenario. We plot the mean values of  $\Delta x^f$  versus the ratio of change of initial longitudinal distance  $\delta$ , with error bands denoting 95% confidence interval.

and trustworthy human cooperation, which helps the model generalize to unseen situations even if it might misinterpret the relations.

Another useful insight we draw from the experiment is that interaction labels are not sufficient to induce an explainable model with semantic latent space. Even though the supervised policy utilizes additional information on the ground-truth interaction graph, it fails to synthesize the following behavior in novel scenarios. Although the GRI model still has a considerable gap in reconstruction performance compared to the supervised baseline, it provides a promising and principled manner to incorporate prior knowledge into a learning-based autonomous driving system and induce an explainable model.

## VII. DISCUSSION AND CONCLUSION

In this work, we propose Grounded Relational Inference (GRI), which models an interactive system’s underlying dynamics by inferring the agents’ semantic relations. By incorporating structured reward functions, we ground the relational latent space into semantically meaningful behaviors defined with expert domain knowledge. Therefore, we assure an interpretable interaction graph at the design stage. We demonstrate that it can model simple traffic scenarios under both simulation and real-world settings, and generate interpretable graphs explaining the vehicle’s behavior by their interactions.

Although we limit our experimental study to the autonomous driving domain, the model itself is formulated without specifying the context. As long as proper domain knowledge is available, the proposed method can be extended naturally to other fields (e.g., human-robot interaction). However, there are several technical gaps we need to bridge before extending the current framework to more complicated traffic scenarios and interactive systems in other fields. One gap between the current model and these practical modules is graph dynamics. Throughout the paper, we assume a static interaction graph over the time horizon. We will investigate how to incorporate dynamic graph modeling into the current framework. Another gap is the cooperative assumption, which we would like to remove in the future so that the framework

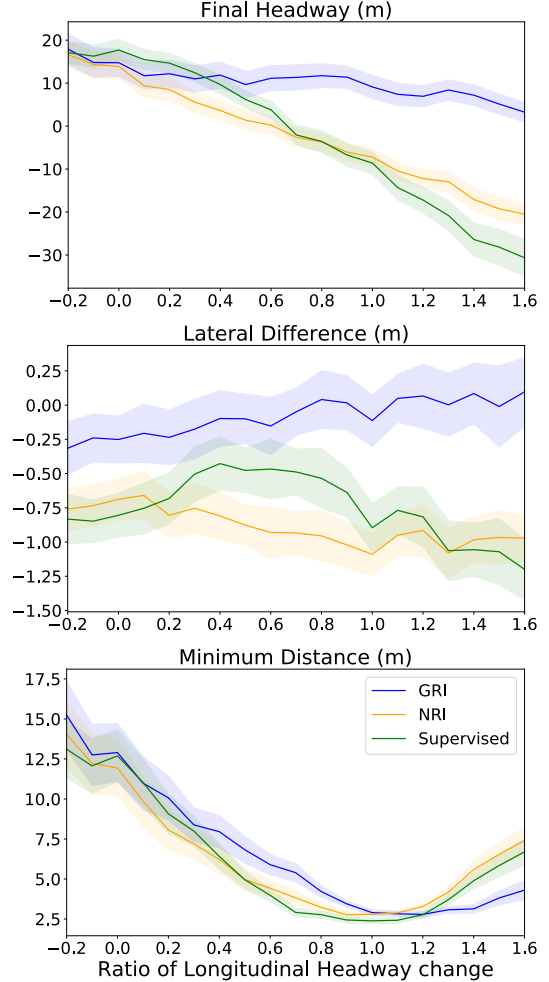


Fig. 11: Results in out-of-distribution naturalistic traffic lane-changing scenario. We plot the mean values of  $\Delta x^f$ ,  $\Delta y$ , and  $d_{\min}$  versus the ratio of change of initial longitudinal distance  $\delta$ , with error bands denoting 95% confidence interval.

can be generalized to non-cooperative scenarios. Besides, as we have mentioned before, the GRI model still has a considerable gap in reconstruction performance compared to the other baselines. In future work, we will improve the model architecture and training algorithm to fill the performance gap while maintaining the advantages of GRI as an explainable model.

## VIII. APPENDIX

### A. Graph Neural Network Model Details

In terms of model structure, both the encoder and the policy decoder are built based on node-to-node message-passing [32], consisting of a node-to-edge message-passing and an edge-to-node message-passing:

$$v \rightarrow e : \mathbf{h}_{i,j}^l = f_e^l(\mathbf{h}_i^l, \mathbf{h}_j^l, \mathbf{x}_{i,j}), \quad (14)$$

$$e \rightarrow v : \mathbf{h}_j^{l+1} = f_v^l(\sum_{i \in \mathcal{N}_j} \mathbf{h}_{i,j}^l, \mathbf{x}_j), \quad (15)$$

where  $\mathbf{h}_i^l$  is the embedded hidden state of node  $v_i$  in the  $l^{\text{th}}$  layer and  $\mathbf{h}_{i,j}^l$  is the embedded hidden state of the edge  $e_{i,j}$ .

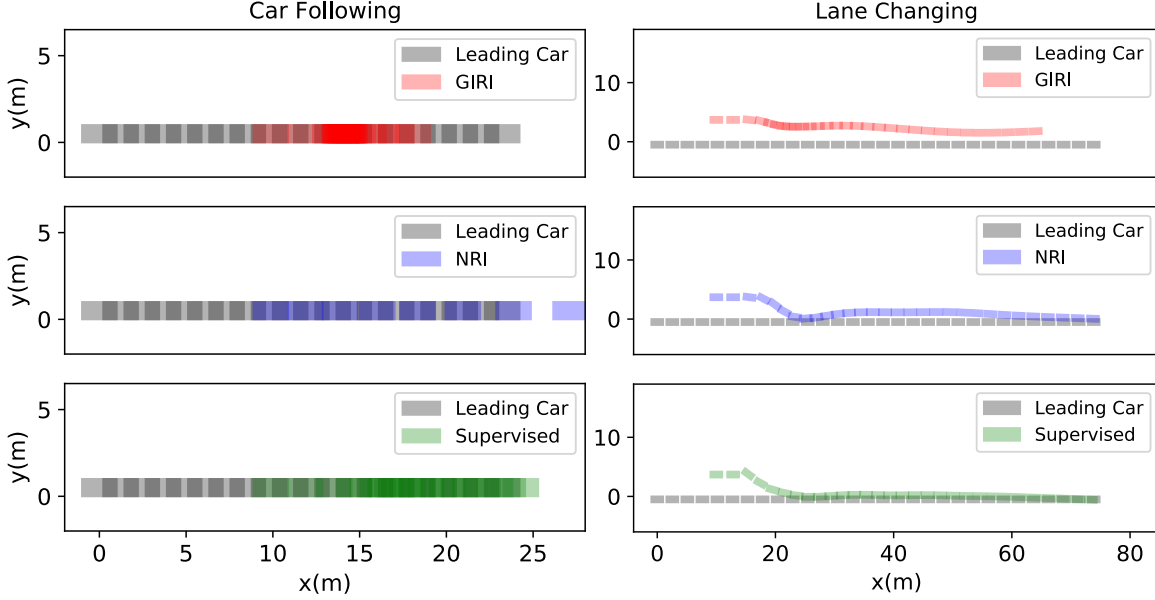


Fig. 12: Examples where the leading car is placed behind the following one at the initial timestep. The trajectories are visualized as a sequences of rectangles. Each rectangle represents a vehicle at a specific time step. The vehicles are driving along the positive direction of the x-axis. The GRI policy still prompts the car-following behavior: It slows down the vehicle until the leading one surpasses it. Meanwhile, the NRI policy and the supervised one do not behave as  $\mathcal{G}_{\text{interact}}$  suggests.

The features  $\mathbf{x}_i$  and  $\mathbf{x}_{i,j}$  are assigned to the node  $v_i$  and the edge  $e_{i,j}$  respectively as inputs.  $\mathcal{N}_j$  denotes the set of the indices of  $v_i$ 's neighbouring nodes connected by an incoming edge. The functions  $f_e^l$  and  $f_v^l$  are neural networks for edges and nodes respectively, shared across the graph within the  $l^{\text{th}}$  layer of node-to-node message-passing.

**GNN Encoder.** The GNN encoder is essentially the same as in NRI. It models the posterior distribution as  $q_\phi(\mathbf{z}|\boldsymbol{\tau})$  with the following operations:

$$\begin{aligned} \mathbf{h}_j^1 &= f_{\text{emb}}(\mathbf{x}_j), \\ v \rightarrow e : \quad \mathbf{h}_{i,j}^1 &= f_e^1(\mathbf{h}_i^1, \mathbf{h}_j^1), \\ e \rightarrow v : \quad \mathbf{h}_j^2 &= f_v^1 \left( \sum_{i \neq j} \mathbf{h}_{i,j}^1 \right), \\ v \rightarrow e : \quad \mathbf{h}_{i,j}^2 &= f_e^2(\mathbf{h}_i^2, \mathbf{h}_j^2), \\ q_\phi(\mathbf{z}_{i,j}|\boldsymbol{\tau}) &= \text{softmax}(\mathbf{h}_{i,j}^2), \end{aligned}$$

where  $f_e^1, f_v^1$  and  $f_e^2$  are fully-connected networks (MLP) and  $f_{\text{emb}}$  is a 1D convolutional networks (CNN) with attentive pooling.

**GNN Policy Decoder.** The policy operates over  $\mathcal{G}_{\text{interact}}$  and models the distribution  $\pi_\eta(\mathbf{a}_j^t|\mathbf{x}^t, \mathbf{z})$ , which can be factorized with  $\pi_\eta(\mathbf{a}_j^t|\mathbf{x}^t, \mathbf{z})$  as in Eqn. (1). We model  $\pi_\eta$  as a Gaussian distribution with the mean value parameterized by the following GNN:

$$v \rightarrow e : \quad \tilde{\mathbf{h}}_{i,j}^t = \sum_{k=0}^K \mathbf{1}(z_{i,j} = k) \tilde{f}_e^k(\mathbf{x}_i^t, \mathbf{x}_j^t), \quad (16)$$

$$e \rightarrow v : \quad \mu_j^t = \tilde{f}_v \left( \sum_{i \neq j} \tilde{\mathbf{h}}_{i,j}^t \right), \quad (17)$$

$$\pi_\eta(\mathbf{a}_j^t|\mathbf{x}^t, \mathbf{z}) = \mathcal{N}(\mu_j^t, \sigma^2 \mathbf{I}). \quad (18)$$

Alternatively, the model capacity is improved by using a recurrent policy  $\pi_\eta(\mathbf{a}_j^t|\mathbf{x}^t, \dots, \mathbf{x}^1, \mathbf{z})$ ; Namely, the agents take actions according to the historical trajectories of the system. We follow the practice in [12] and add a GRU unit to obtain the following recurrent model:

$$v \rightarrow e : \quad \tilde{\mathbf{h}}_{i,j}^t = \sum_{k=0}^K \mathbf{1}(z_{i,j} = k) \tilde{f}_e^k \left( \tilde{\mathbf{h}}_i^t, \tilde{\mathbf{h}}_j^t \right), \quad (19)$$

$$e \rightarrow v : \quad \tilde{\mathbf{h}}_j^{t+1} = \text{GRU} \left( \sum_{i \neq j} \tilde{\mathbf{h}}_{i,j}^t, \mathbf{x}_j^t, \tilde{\mathbf{h}}_j^t \right), \quad (20)$$

$$\mu_j^t = f_{\text{out}} \left( \tilde{\mathbf{h}}_j^{t+1} \right), \quad (21)$$

$$\pi_\eta(\mathbf{a}_j^t|\mathbf{x}^t, \dots, \mathbf{x}^1, \mathbf{z}) = \mathcal{N}(\mu_j^t, \sigma^2 \mathbf{I}), \quad (22)$$

where  $\tilde{\mathbf{h}}_i^t$  is the recurrent hidden state encoding the historical information up to the time step  $t-1$ .

## REFERENCES

- [1] M. Bojarski, D. Del Testa, D. Dworakowski, B. Firner, B. Flepp, P. Goyal, L. D. Jackel, M. Monfort, U. Muller, J. Zhang, *et al.*, “End to end learning for self-driving cars,” *arXiv preprint arXiv:1604.07316*, 2016.
- [2] X. Chen, H. Ma, J. Wan, B. Li, and T. Xia, “Multi-view 3d object detection network for autonomous driving,” in *Proceedings of the IEEE Conference on Computer Vision and Pattern Recognition (CVPR)*, 2017, pp. 1907–1915.
- [3] C. Tang, Z. Xu, and M. Tomizuka, “Disturbance-Observer-Based Tracking Controller for Neural Network Driving Policy Transfer,” *IEEE Transactions on Intelligent Transportation Systems*, 2019.
- [4] A. B. Arrieta, N. Díaz-Rodríguez, J. Del Ser, A. Bennetot, S. Tabik, A. Barbado, S. García, S. Gil-López, D. Molina, R. Benjamins, *et al.*, “Explainable artificial intelligence (xai): Concepts, taxonomies, opportunities and challenges toward responsible ai,” *Information Fusion*, vol. 58, pp. 82–115, 2020.

[5] J. Kim and J. Canny, "Interpretable learning for self-driving cars by visualizing causal attention," in *Proceedings of the IEEE international conference on computer vision (ICCV)*, 2017, pp. 2942–2950.

[6] M. Bojarski, A. Choromanska, K. Choromanski, B. Firner, L. J. Ackel, U. Müller, P. Yeres, and K. Zieba, "Visualbackprop: Efficient visualization of cnns for autonomous driving," in *2018 IEEE International Conference on Robotics and Automation (ICRA)*. IEEE, 2018, pp. 1–8.

[7] A. Alahi, K. Goel, V. Ramanathan, A. Robicquet, L. Fei-Fei, and S. Savarese, "Social lstm: Human trajectory prediction in crowded spaces," in *Proceedings of the IEEE Conference on Computer Vision and Pattern Recognition (CVPR)*, 2016, pp. 961–971.

[8] A. Vemula, K. Muelling, and J. Oh, "Social attention: Modeling attention in human crowds," in *2018 IEEE international Conference on Robotics and Automation (ICRA)*. IEEE, 2018, pp. 1–7.

[9] Y. Hoshen, "Vain: Attentional multi-agent predictive modeling," in *Advances in Neural Information Processing Systems (NIPS)*, 2017, pp. 2701–2711.

[10] P. Veličković, G. Cucurull, A. Casanova, A. Romero, P. Lio, and Y. Bengio, "Graph attention networks," *International Conference on Learning Representations (ICLR)*, 2018.

[11] S. Sukhbaatar, A. Szlam, and R. Fergus, "Learning multiagent communication with backpropagation," in *Advances in Neural Information Processing Systems (NIPS)*, 2016, pp. 2244–2252.

[12] T. Kipf, E. Fetaya, K.-C. Wang, M. Welling, and R. Zemel, "Neural relational inference for interacting systems," *International Conference on Machine Learning (ICML)*, 2018.

[13] L. Sun, W. Zhan, and M. Tomizuka, "Probabilistic prediction of interactive driving behavior via hierarchical inverse reinforcement learning," in *2018 21st International Conference on Intelligent Transportation Systems (ITSC)*. IEEE, 2018, pp. 2111–2117.

[14] D. Lee, Y. Gu, J. Hoang, and M. Marchetti-Bowick, "Joint interaction and trajectory prediction for autonomous driving using graph neural networks," *arXiv preprint arXiv:1912.07882*, 2019.

[15] S. Van Steenkiste, M. Chang, K. Greff, and J. Schmidhuber, "Relational neural expectation maximization: Unsupervised discovery of objects and their interactions," *International Conference on Learning Representations (ICLR)*, 2018.

[16] P. Battaglia, R. Pascanu, M. Lai, D. J. Rezende, et al., "Interaction networks for learning about objects, relations and physics," in *Advances in Neural Information Processing Systems (NIPS)*, 2016, pp. 4502–4510.

[17] L. Yu, J. Song, and S. Ermon, "Multi-agent adversarial inverse reinforcement learning," *International Conference on Learning Representations (ICLR)*, 2019.

[18] R. P. Bhattacharyya, D. J. Phillips, B. Wulfe, J. Morton, A. Kuefler, and M. J. Kochenderfer, "Multi-agent imitation learning for driving simulation," in *2018 IEEE/RSJ International Conference on Intelligent Robots and Systems (IROS)*. IEEE, 2018, pp. 1534–1539.

[19] J. Ho and S. Ermon, "Generative adversarial imitation learning," in *Advances in Neural Information Processing Systems (NIPS)*, 2016, pp. 4565–4573.

[20] R. P. Bhattacharyya, D. J. Phillips, C. Liu, J. K. Gupta, K. Driggs-Campbell, and M. J. Kochenderfer, "Simulating emergent properties of human driving behavior using multi-agent reward augmented imitation learning," in *2019 International Conference on Robotics and Automation (ICRA)*. IEEE, 2019, pp. 789–795.

[21] Z. Wang, J. S. Merel, S. E. Reed, N. de Freitas, G. Wayne, and N. Heess, "Robust imitation of diverse behaviors," in *Advances in Neural Information Processing Systems (NIPS)*, 2017, pp. 5320–5329.

[22] X. B. Peng, A. Kanazawa, S. Toyer, P. Abbeel, and S. Levine, "Variational discriminator bottleneck: Improving imitation learning, inverse rl, and gans by constraining information flow," *International Conference on Learning Representations (ICLR)*, 2019.

[23] L. Yu, T. Yu, C. Finn, and S. Ermon, "Meta-inverse reinforcement learning with probabilistic context variables," in *Advances in Neural Information Processing Systems (NIPS)*, 2019, pp. 11772–11783.

[24] J. Kim, A. Rohrbach, T. Darrell, J. Canny, and Z. Akata, "Textual explanations for self-driving vehicles," in *Proceedings of the European conference on computer vision (ECCV)*, 2018, pp. 563–578.

[25] P. de Haan, D. Jayaraman, and S. Levine, "Causal confusion in imitation learning," in *Advances in Neural Information Processing Systems (NIPS)*, 2019, pp. 11698–11709.

[26] C. Li, S. H. Chan, and Y.-T. Chen, "Who make drivers stop? towards driver-centric risk assessment: Risk object identification via causal inference," *arXiv preprint arXiv:2003.02425*, 2020.

[27] B. D. Ziebart, A. Maas, J. A. Bagnell, and A. K. Dey, "Maximum entropy inverse reinforcement learning," in *Proceedings of AAAI Conference on Artificial Intelligence*, 2008.

[28] C. Finn, S. Levine, and P. Abbeel, "Guided cost learning: Deep inverse optimal control via policy optimization," in *International Conference on Machine Learning (ICML)*, 2016, pp. 49–58.

[29] C. Finn, P. Christiano, P. Abbeel, and S. Levine, "A connection between generative adversarial networks, inverse reinforcement learning, and energy-based models," *arXiv preprint arXiv:1611.03852*, 2016.

[30] J. Fu, K. Luo, and S. Levine, "Learning robust rewards with adversarial inverse reinforcement learning," *arXiv preprint arXiv:1710.11248*, 2017.

[31] A. Kesting, M. Treiber, and D. Helbing, "Enhanced intelligent driver model to access the impact of driving strategies on traffic capacity," *Philosophical Transactions of the Royal Society A: Mathematical, Physical and Engineering Sciences*, vol. 368, no. 1928, pp. 4585–4605, 2010.

[32] J. Gilmer, S. S. Schoenholz, P. F. Riley, O. Vinyals, and G. E. Dahl, "Neural message passing for quantum chemistry," in *Proceedings of the 34th International Conference on Machine Learning (ICML)-Volume 70*. JMLR. org, 2017, pp. 1263–1272.

[33] A. A. Alemi, I. Fischer, J. V. Dillon, and K. Murphy, "Deep variational information bottleneck," *International Conference on Learning Representations (ICLR)*, 2017.

[34] I. Higgins, L. Matthey, A. Pal, C. Burgess, X. Glorot, M. Botvinick, S. Mohamed, and A. Lerchner, "beta-vae: Learning basic visual concepts with a constrained variational framework," *International Conference on Learning Representations (ICLR)*, 2017.

[35] S. Levine, "Reinforcement learning and control as probabilistic inference: Tutorial and review," *arXiv preprint arXiv:1805.00909*, 2018.

[36] M. Treiber, A. Hennecke, and D. Helbing, "Congested traffic states in empirical observations and microscopic simulations," *Physical review E*, vol. 62, no. 2, p. 1805, 2000.